Study of the electrocatalytic hydrogenation of benzaldehyde and furfural at heterostructured MoS_2/N-carbon thin film electrodes

Christian Schröder,[1] Hugo Nolan,[1,2] Lua Henderson,[1] Paula E. Colavita[1,2*]

1- School of Chemistry, Trinity College Dublin, Dublin D02PN40, Ireland

2- CRANN and AMBER Research Centres, Trinity College Dublin, Dublin D02 PN40, Ireland

[*] Corresponding author contact: colavitp@tcd.ie

Abstract

Electrocatalytic hydrogenation (ECH) has been proposed as a route to sustainable organic hydrogenations, however development of low-cost and sustainable electrocatalyst materials for this reaction is still needed. Herein, we investigate thin film heterostructured electrodes consisting of MoS_2 supported at N-doped carbon in the ECH of carbonylated organics. Carbon-supported MoS_2 is known to catalyse the hydrogen evolution reaction, however its potential to activate hydrogen towards organic hydrogenations is poorly understood. Electrodes were fabricated using a combination of sputter deposition, thermal treatments and CVD proximity growth, yielding thin film electrodes with well-defined geometry, morphology and N-functionality type. MoS_2/N-carbon films were characterized via microscopy, Raman and X-ray absorption spectroscopy. Electrochemical methods were used to establish the loading of electroactive Mo-centers and quantitatively assess their activity. The response of MoS_2/N-carbon as electrocatalyst in the ECH was first investigated via voltammetry and electrolysis using benzaldehyde as a diagnostic carbonylated compound. The turnover frequency (TOF) at Mo-centers was estimated to be *ca.* 600 h^{-1} in 20 mM solutions at -0.6 V vs RHE, with 97% selectivity towards the alcohol vs the electrodimerization product. Performances were then studied using furfural, a substrate of interest for ECH applications to the stabilization of bio-oil. TOF of *ca.* 900 h^{-1} were obtained with 94% alcohol selectivity under the same conditions and, notably, no evidence of over-hydrogenation, a common problem in the ECH of furfural. These results suggest that MoS_2/N-carbon materials hold potential to deliver competitive performances compared to precious metal electrocatalysts in the literature.

Keywords: molybdenum disulfide, electrocatalytic hydrogenation, furfural, transition metal dichalcogenides, electrocatalysis

Introduction

Electrocatalytic hydrogenation (ECH) is a promising alternative for lowering the carbon footprint of hydrogenations, that also holds potential to enable safer and decentralized synthesis of chemicals and fuels.[1-5] Hydrogenation reactions are ubiquitous in industrial chemistry and play an important role in the synthesis of fine chemicals and hydrocarbon feedstocks,[6, 7] as well as in proposed routes to upgrading of waste or by-product streams.[8] Conventional hydrogenation is typically carried out under conditions of high temperature and high H_2 pressure in the presence of precious metal catalysts.[7] While good selectivity and yields can be achieved, such reactions are energy intensive and require the use of scarce and/or expensive metals and high purity H_2, which is typically sourced from fossil fuels. In the ECH, hydrogen is instead produced *in situ*, under ambient conditions via electroreduction of protons/water in aqueous electrolyte.[9] Coupling the ECH to electricity from renewable energy can thus lower the energy input and carbon emissions associated with hydrogenations compared to conventional processes. This has prompted significant interest in exploring ECH routes for key hydrogenation reactions including the hemi-hydrogenation of ethyne,[10] N_2 hydrogenation to ammonia[11-13] and, particularly, hydrorefining of bio-oil.[3, 8]

In the case of this last reaction, ECH has been proposed as an economically viable route to reducing carbonyl groups responsible for instability of pyrolysis oils, while increasing its energy density for fuel applications.[4, 14] However, to realise the potential of ECH in this application, further development of low-cost electrocatalyst materials is still needed. As the ECH requires the generation of adsorbed hydrogen H_{ads} at the catalyst via the Volmer step ($H^+ + e \rightarrow H_{ads}$), metals with activity in the HER can be potentially good electrocatalysts for the ECH, as long as competition between these two processes can be controlled. Indeed, Pd, Pt and other Pt-group metals have been shown to display good activity in the ECH of carbonyl groups to alcohols.[2, 15-22] However, their scarcity and cost, coupled to their susceptibility

towards poisoning make them less attractive in applications to biomass or waste streams. Copper-based electrocatalyst have been studied as lower cost alternatives, however copper tends to catalyse hydrogenation and C—C coupling[14, 23-25] which can present challenges for selectivity and consequent separation costs. Carbonylated compounds, namely benzaldehyde and furfural are often used in the investigation of the ECH.[17, 18, 20, 26-28] While benzaldehyde serves often as a diagnostic compound to characterise electrocatalysts, furfural is of interest in biomass valorisations, as its hydrogenation products can find application in several industrial processes.[29, 30]

In this work we investigate the performance of MoS_2/carbon heterostructured electrodes in the ECH of carbonyl compounds. MoS_2 is a layered material that has been extensively studied as an electrocatalyst for the hydrogen evolution reaction (HER)[31, 32] and CO_2 reductions,[33, 34] but that has received limited attention as a possible material for the ECH of organics.[35] Recent work from our group[36] reported on the synthesis of MoS_2 nanoparticle thin films onto N-doped graphitized carbon electrodes via chemical vapour deposition (CVD) methods. The resulting MoS_2/N-carbon heterostructured thin film electrodes were found to display high activity in the HER, while displaying a well-defined geometry and nanostructure that facilitates interpretation of their electrochemical response. Importantly, the presence and type of N-functionalities in the carbon support were found to modulate HER activity through substrate-MoS_2 interactions. Herein, we use these materials to investigate potential applications of MoS_2/N-carbon as an electrocatalyst for the ECH conversion of carbonyls to alcohols. To this end, benzaldehyde was first chosen as a diagnostic substrate and a surrogate for aromatic carbonyl compounds present in bio-oil. **Scheme 1** shows chemical steps involved in the ECH of benzaldehyde, which is known to yield two possible products: benzyl alcohol and the dimerized product hydrobenzoin.[14, 23, 25, 37] Therefore this reaction offers an opportunity to investigate drivers of selectivity as well as of activity. Further, the ECH of benzaldehyde has been studied using a

range of metal electrocatalysts thus enabling quantitative benchmarking of performance indicators, as discussed in this work.

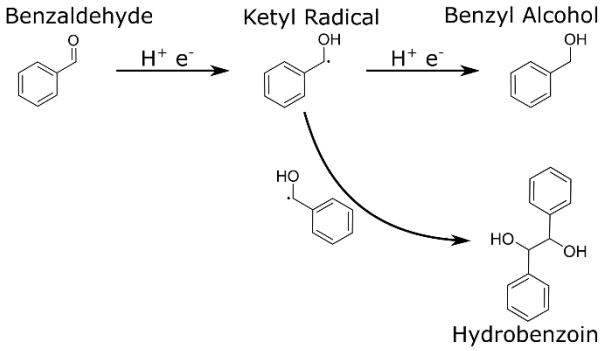

Scheme 1. Reaction pathways of the ECH of benzaldehyde.

To the best of our knowledge there are no reports of the ECH of benzaldehyde using MoS_2/carbon electrodes. MoS_2 readily catalyses H_{ads} activation and H_2 evolution whereas graphitic carbons are poor at stabilizing H_{ads}; on the other hand, benzaldehyde is expected to adsorb with similar binding strength at both of these materials.[23] We therefore hypothesized that fabrication of MoS_2/N-carbon composites might offer opportunities to regulate activity and selectivity in the ECH of carbonylated compounds, as suggested by few ECH studies using Pt-group metals.[38] Further, we expanded the substrate scope to furfural, a compound of specific interest for biomass valorization via ECH.[27, 39] Our results indicate that these materials can display high turnover frequency (TOF) values and good selectivity towards the alcohol product through potential control using carbonylated compounds of interest for both benchmarking and practical application purposes.

Experimental

Sulfuric acid (99.999%), MoO_3 (Reagent Plus, >99.5%), isopropanol (HPLC, 99.9%), sulfur (Aldrich, 99.98%), acetophenone (Sigma Aldrich, Reagent Plus 99%), ethyl acetate (Sigma

Aldrich, HPLC Plus, 99.9 %), benzaldehyde (Reagent Plus ≥99%) and furfural (98%) were used as received. Glassy carbon (GC) plates (Sigradur, 2×1 cm^2) were purchased from Hochtemperatur-Werkstoffe GmbH. Nitrogen (99.998%, OFN) and argon (99.998%, Pureshield) were purchased from BOC. Graphite targets (99.999%) were obtained from Kurt J. Lesker.

GC was polished prior to deposition and/or characterization using previously published procedures:[36] 1200 grit sandpaper was used first, followed by alumina slurries of 1 and 0.3 µm size on nylon cloth pads (Buehler), and 0.3 and 0.05 µm size on Microcloth pads (Buehler); substrates were sonicated and rinsed between polishing steps. The final polishing step was carried out immediately before use to ensure a clean surface. Nitrogenated carbon films were synthesised as previously reported.[40] Briefly, amorphous thin films were first deposited in a dc-magnetron sputtering chamber with <2 $\times 10^{-6}$ mbar base pressure, using a graphite target and 2% N_2/Ar (by flow) at 50 sccm (1-2 $\times 10^{-2}$ mbar deposition pressure) for 40 min. These amorphous films were then graphitised at 900 °C under N_2 flow in a tube furnace (Carbolite Gero) yielding nitrogenated graphitized films, referred to as anC:N_G in this work.

MoS_2 films were grown via CVD following a previously reported method.[36] 50 µL/cm^2 of a 1 mg/mL MoO_3 dispersion in isopropanol were drop-cast on a Si wafer to form a "seed" layer; substrates were placed face-down on the wafers, forming a microreactor in the volume between the seed and growth surfaces. This assembly was placed in a quartz tube furnace and heated to 750 °C under Ar (125 sccm); sulfur powder was sublimed at 120 °C in an upstream secondary heating zone for 20 min. Vaporized MoO_3 reacted with sulfur in the microreactor volume resulting in the deposition of MoS_2 onto the growth substrate, namely SiO_2, anC:N_G films or GC, as specified in each case. Samples were cooled to room temperature under Ar flow.

Raman spectroscopy was carried out using a confocal scanning Raman system (Witec alpha 300R) at 532 nm excitation; spectral analysis was performed using commercial software (Witec Project 5.1). X-ray diffraction (XRD) was carried out using a D2 Phaser diffractometer with LynxEye detector (Bruker) and a Cu Kα source. X-ray photoelectron spectroscopy (XPS) was carried out in an Omicron ESCA system with a XM1000MK II monochromated Al Kα X-ray source (1486.7 eV) and an EA 125 analyzer. Survey scans and high-resolution spectra were obtained with 50 and 15 eV pass energies, respectively. Best-fits were obtained with Gaussian-Lorentzian peaks, after Shirley background correction, using CasaXPS software; energy values are referenced to the C 1s peak (284.8 eV). Elemental compositions were calculated from peak area ratios after correction for relative sensitivity factors. Transmission electron microscopy (TEM) was carried on a JEOL 2100 LaB TEM with 200 kV accelerating voltage. Samples for TEM were prepared by delaminating the MoS_2/anC:N_G films from a Si wafer using a razor blade; film sections were then transferred onto a gold grid (Ted Pella Inc., 200 mesh carbon film).

Electrochemical voltammetry studies were carried out in a three-electrode cell using a graphite rod as counter electrode, modified GC disks as working electrodes and Ag/AgCl as reference electrode (IJ Cambria). 0.1 M H_2SO_4 was used as supporting electrolyte for all measurements unless otherwise noted; all solutions were prepared with 18.2 MΩ deionised water and purged with N_2 for 20 min prior to any measurements. Electrolysis studies were carried out using a glass H-cell with anodic and cathodic compartments separated by a conductive membrane (Nafion, 0.002 in.). The anodic compartment contained the counter electrode and supporting electrolyte, while the cathodic compartment contained the working and reference electrodes in supporting electrolyte with added benzaldehyde. Potentiostatic electrolysis experiments were carried out by applying a defined potential for 30 min under stirring (500 rpm) at 25°C. Product analysis was carried out using a gas chromatography system (GC8860, Agilent) equipped with

a flame ionisation detector, capillary column (DB Wax, Agilent) and H_2 as carrier gas. 2 mL of the electrolyte were taken and an internal standard of acetophenone added; organics were extracted with 2 mL of ethyl acetate and analysed at 2 mL/min flow using 1 µL of the organic phase for injection (split injection, 10:1). Figures of merit were calculated using the expressions summarized in **Supporting Information**.

Results and Discussion

Previous work from our group demonstrated the synthesis of MoS_2 nanoparticle film electrodes supported onto graphitized nitrogenated carbon (anC:N_G) using a procedure schematically illustrated in **Figure 1a.**[36] Nitrogenated carbon thin films were first obtained via a two-step process, consisting of sputter deposition followed by thermal annealing under inert atmosphere. anC:N_G films are approximately 65 nm thick, display a well graphitized matrix, N/C of 3.2 at.% low roughness (R_q <1.5 nm), and a homogeneous structure and composition, as discussed in greater detail in our previous work.[36, 40] The MoS_2 nanoparticle film was grown onto anC:N_G via proximity CVD as described in the experimental section.[41] **Figure 1b and 1c** show optical and TEM microscopy images, respectively, of MoS_2/anC:N_G, fabricated on a GC plate support. The optical image shows regions of higher and lower MoS_2 density, which appear as brighter and darker in optical contrast. TEM characterization indicates that MoS_2 films are polycrystalline and consist of closely packed nanoparticles (53 ± 8 nm in size) supported onto the anC:N_G underlayer. The layered structure of MoS_2 is evident from images of selected crystallites, **Figure S1,** with observed spacing of 0.71 ± 0.01 nm, slightly larger than the literature value of 0.65 nm.[42] *d*-spacings obtained from the selected area electron diffraction (SAED) pattern of MoS_2/anC:N_G, **Figure S1** and **Table S1**, are consistent with the (1 0 0) and (1 0 1) reflections of 2H-MoS_2 (PDF 37-1492). Reflections associated with (2 1 0) and (2 1 1) of MoO_2 (PDF 32-0671) are also detectable as minor contributions.

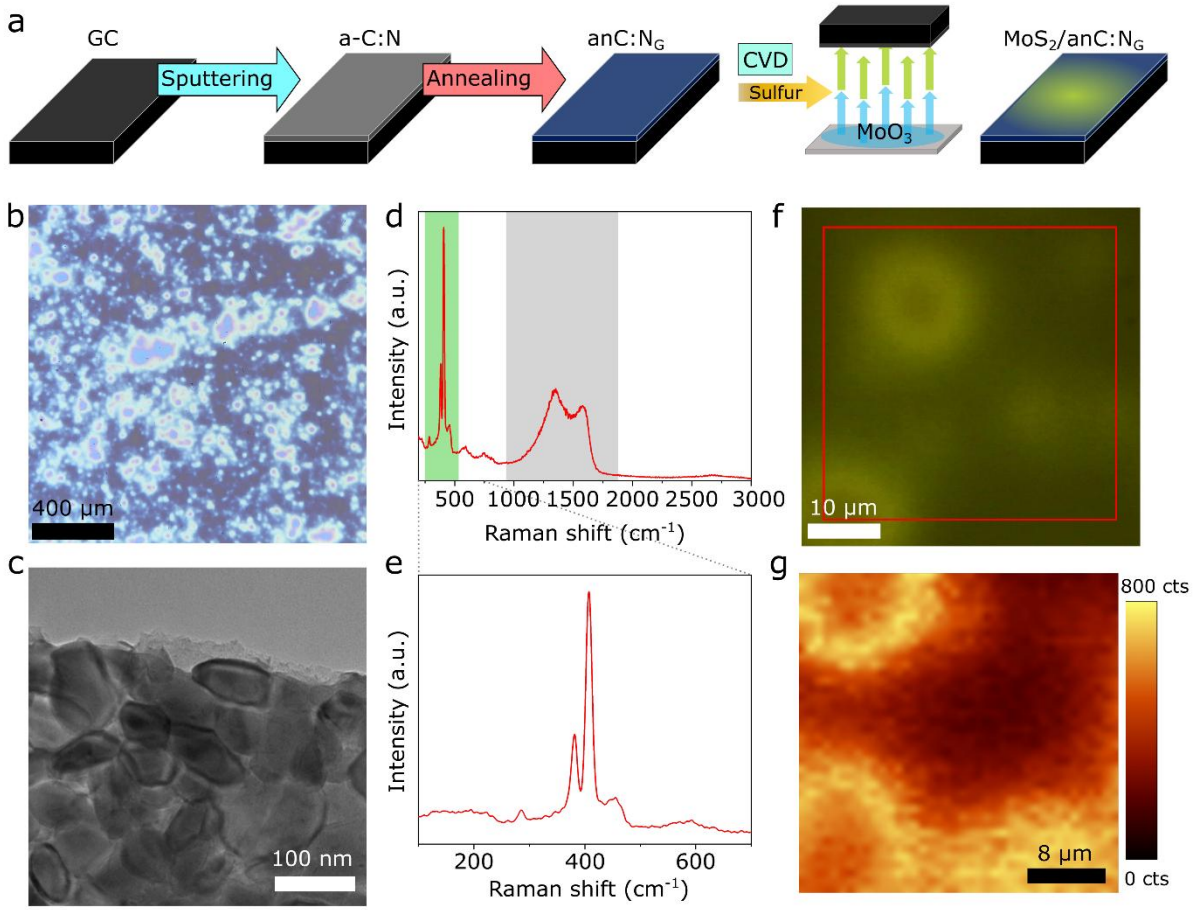

Figure 1. (a) Scheme of synthetic steps involved in the fabrication of MoS_2/anC:N_G heterostructures. (b) Optical microscopy of MoS_2 film grown on an-C:N_G on a GC plate (×140 magnification). (c) TEM image of MoS_2/an-C:N_G film showing both nanoparticles and the graphitized carbon support layer. (d) Representative Raman spectrum of MoS_2/anC:N_G film; spectral regions characteristic of MoS_2 and carbon materials are highlighted in green and gray, respectively. (e) Details of the Raman spectrum in the MoS_2 diagnostic region, from data in (d). (f) Optical image of MoS_2/anC:N_G in the area used for the Raman intensity mapping shown in (g); the intensity map was obtained by integrating peaks in the 350-450 cm^{-1} spectral region so that brighter areas indicate higher Raman scattering intensity from MoS_2 nanoparticles.

MoS_2 growth was further confirmed via Raman spectroscopy/microscopy. A representative spectrum of MoS_2/anC:N_G electrodes is shown in **Figure 1d**: the MoS_2 characteristic doublet arising from Mo and S displacements from the *c* axis is observed at *ca.* 385 and 413 cm^{-1},[43] while the D and G bands typical of graphitic carbons are also observed at *ca.* 1358 and 1593 cm^{-1}, respectively. The MoS_2 spectrum, shown in greater detail in **Figure 1e**, is consistent with that of the 2H-MoS_2 phase, as the peak manifold at rel. shift below 350 cm^{-1} and

characteristic of 1T'-MoS_2 is absent,[44] in agreement with results from TEM and XRD of the composite thin films, **Figure S2**. Spectra in **Figure 1e** also support that the nanoparticle film undergoes surface sulfidation, as only a weak contribution from the MoO_3 peak at 285 cm^{-1} can be detected while characteristic peaks of MoO_2 at 363 and 495 cm^{-1} are not observed.[45] A Raman map of the total intensity of the MoS_2 signal (**Figure 1f and 1g)** indicated that MoS_2 covers the entire anC:N_G surface but it is distributed with selected regions of higher concentration, as indicated by the intensity contrast.

Composition of heterostructured films was first investigated via XPS. The survey spectrum, **Figure 2a**, shows peaks corresponding to C 1s (*ca.* 284 eV), O 1s (*ca.* 532 eV), N 1s (*ca.* 400 eV), Mo 3p (*ca.* 390 eV), Mo 3d (*ca.* 230 eV) and S 2p (*ca.* 164 eV). Best-fits of the Mo 3d and S 2p regions in **Figure 2b and 2c**, respectively, indicate that spectra are consistent with Mo^{+4} and S^{-2} species contributing to the majority of the intensity, in agreement with previously reported results for this type of MoS_2/anC:N_G samples.[36] Additional spectra in the C 1s and O 1s region and a summary of results from best-fits are reported in **Figure S3** and **Table S1**. Atomic composition values indicate that the Mo^{+4}/C atomic %-ratio is *ca.* 38% and thus supports a high MoS_2 coverage present at the anC:N_G surface, in agreement with microscopy results in **Figure 1**. However, XPS does not provide information on the fraction of MoS_2 that is electrochemically active and available for electrocatalysis. Therefore, the electrochemically active loading of MoS_2 at CVD grown MoS_2/anC:N_G electrodes was obtained via voltammetry over a potential window where Mo undergoes electrooxidation. **Figure 2d** shows representative first and second voltametric cycles in 0.1 M H_2SO_4 at 2 mV/s of a MoS_2/anC:N_G electrode. The voltammograms show the presence of an irreversible anodic peak at *ca.* 0.5 V vs Ag/AgCl that is absent from the second cycle and has previously been attributed, as discussed by Bonde et al.,[31] to the 11-electron process:

$$MoS_2 + 7\,H_2O \rightarrow MoO_3 + SO_4^{2-} + {}^1/_2\,S_2^{2-} + 14H^+ + 11e^- \qquad \text{(eq.1)}$$

The total integrated charge associated with the peak was therefore used to obtain an estimate of the surface density of electrochemically active MoS_2, yielding $(5.2 \pm 0.6)\times10^{-9}$ mol/cm^2 (standard error on the mean, N = 34), equivalent to 0.8 µg/cm^2. Taking into account that the areal density in MoS_2 monolayers is 1.9×10^{-9} mol/cm^2,[46, 47] the experimentally determined coverage suggests that the electrochemically active specific surface area is *ca.* 2.5 times the geometric area of the electrode. Also, given the size of MoS_2 crystallites observed via TEM, it is possible to conclude that only the molybdenum atoms located in the top-most layers of the crystallites are available to participate in electrochemical reactions. Finally, no anodic peaks were observed at *ca.* 0.25 V that could arise from surface MoO_2;[48, 49] this indicates that residual MoO_2 is electrochemically inactive and likely present only at the core of nanoparticles.

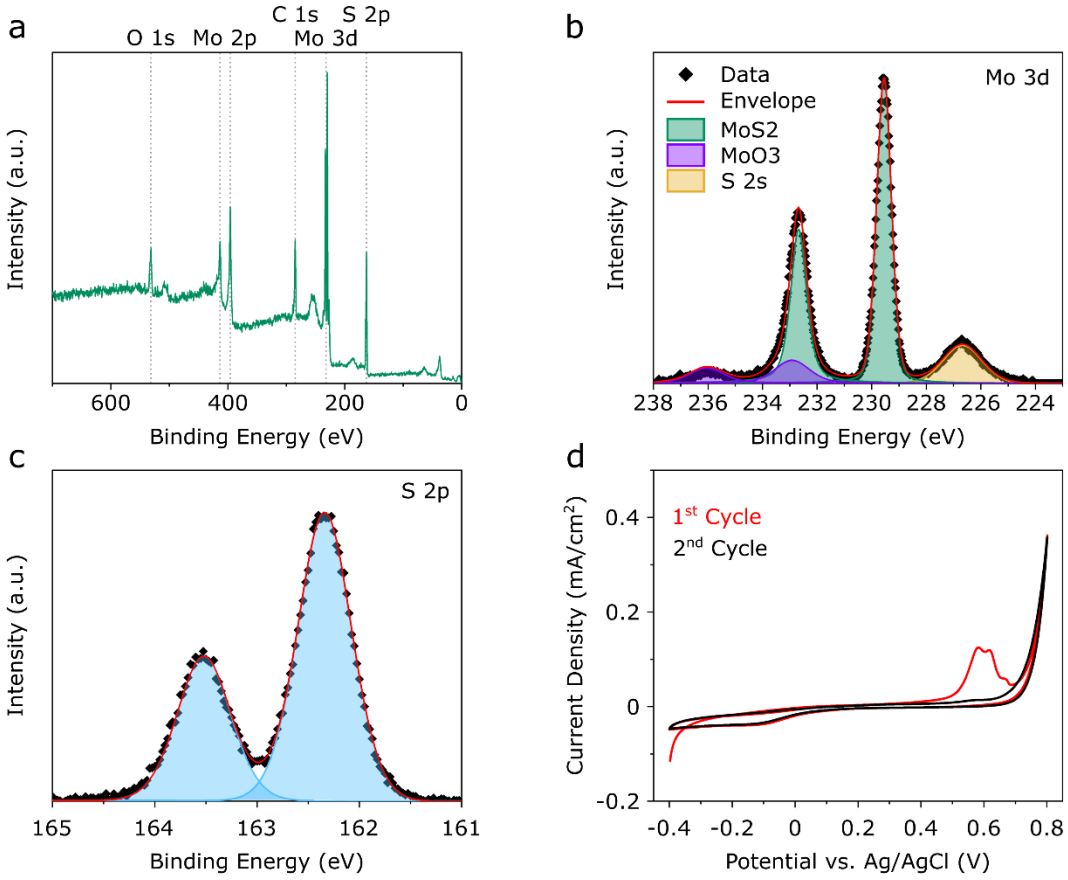

Figure 2. (a) XPS survey spectrum for MoS_2/anC:N_G, high resolution spectra and best fits obtained for (b) Mo 3d and (c) S 2p spectra. (d) Characteristic CV of electrooxidation of MoS_2 in 0.1 M H_2SO_4 at 2 mV/s.

The performance of MoS_2/anC:N_G electrodes in the ECH of unsaturated organics was first investigated via voltammetry. **Figure 3** shows linear sweep voltammograms obtained at 2 mV/s in 0.1 M H_2SO_4 is the absence and presence of 10 mM benzaldehyde (BZH); the response of anC:N_G electrodes is also shown for comparison. In supporting electrolyte alone, the cathodic currents are associated with the hydrogen evolution reaction (HER); this reaction is, as expected, sluggish on anC:N_G electrodes[36, 50, 51] and requires large overpotentials albeit slightly lower than at a conventional GC electrode, as shown in **Figure S4.** On the other hand, MoS_2/anC:N_G show good activity in the HER as indicated by significant reduction of the overpotential needed to observe high cathodic current densities. In the presence of benzaldehyde, the cathodic current at MoS_2/anC:N_G is significantly suppressed, in agreement with the formation of an adsorbed organic layer that blocks HER-active sites, as previously reported for other electrode materials.[20, 37, 52] At the bare anC:N_G electrode, the HER suppression is less pronounced, while in the presence of benzaldehyde it is possible to observe a cathodic peak at *ca.* -0.7 V vs. RHE that is similar to the response obtained at a polished GC disk (**Figure S4**).

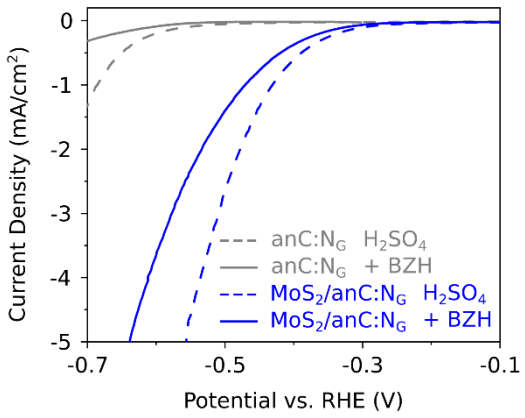

Figure 3. Linear sweep voltammetry at a scan rate of 2 mV/s on anC:N_G (grey) and MoS_2/anC:N_G (blue) in 0.1 M H_2SO_4 (dashed) and with added 10 mM benzaldehyde (solid).

Potentiostatic experiments followed by product analysis were carried out on MoS_2/anC:N_G electrodes to assess activity in the BZH hydrogenation. **Figure 4a** shows representative chronoamperograms obtained under stirring; the cathodic currents decay rapidly and stabilize within the first 10 min at values that progressively increase with increasing overpotential. An exception is the chronoamperogram obtained at -0.7 V vs. RHE which shows irregularities in the trace due to significant gas evolution at this applied potential. Product separation and quantitation at the catholyte were then used to calculate performance indicators; all reactions were carried out over 30 min with conversions remaining <5% so that constant reactant concentrations can be assumed in the reaction vessel. **Figure 4b** shows product rates for the alcohol and the dimerization product: the hydrogenation rate is low at -0.6 V but increases vs overpotential, with the preferred product being benzyl alcohol. The hydrogenation activity observed arises from the MoS_2 phase, as the production rate at either GC or anC:N_G is negligible (**Figure S5)** when compared to those in **Figure 4b**. Further, the MoS_2 phase was found to be chemically stable under the electrolysis conditions, as shown by post-mortem Raman characterization (**Figure S6**). The production of hydrobenzoin is favoured only at potentials more cathodic than -0.6 V vs RHE. At -0.7 V vs RHE the production rate for the dimerization overtakes that of benzyl alcohol, as also evident from **Figure 4c,** which shows alcohol selectivity trends over the potential window explored. A similar decrease in alcohol selectivity can be observed at bare carbon surfaces at the most cathodic overpotentials tested, **Figure S5**.

The faradaic efficiency of BZH hydrogenation, **Figure 4d**, was found to increase from <5% to *ca.* 12% at -0.7 V vs. RHE. These FE values are comparable to those reported by Huang et al.[35] for the hydrogenation of furfural (~11.5%) using MoS_2 on carbon cloth at similar potentials (*ca.* -0.75 V vs RHE) under galvanostatic conditions. It is interesting however to note that the increase in FE is the result of increased alcohol production only at potentials ≥ - 0.6 V vs RHE,

while below this value the majority of the hydrogenation charge leads to hydrobenzoin production, as also indicated by the selectivity trends. The increased dimerization rates and FE, which go hand in hand with decreased selectivity towards benzyl alcohol, suggest potential-dependent changes in the hydrogenation mechanism. Finally, we note that the relatively low values of FE observed are consistent with the high activity of MoS_2 as an HER electrocatalyst; indeed, the mole balance for all reactions was *ca.* 100% (**Figure S7**) thus supporting that the balance of the total charge resulted in hydrogen evolution rather than side electrochemical reactions of BZH.

To compare the performance of MoS_2/an-C:N_G electrocatalysts against others in the literature it is possible to normalize the total hydrogenation rates, in **Figure 4e**, to the surface loading of MoS_2 obtained from electrooxidation, thus yielding estimates of TOF values. This approach is further supported by control experiments in **Figure S5** that showed that contributions to the hydrogenation currents from carbon sites in the support are negligible and that MoS_2 sites can be assumed to be solely responsible for the ECH activity. **Figure 4f** shows trends of TOF vs applied potential; the figure shows an expanded region at low overpotential for clarity, while the full range of the TOF axis is shown in **Figure S8**. It is evident that TOF values undergo a step change between -0.6 and -0.7 V vs RHE leading to a ten-fold increase that supports a change in reaction pathway.

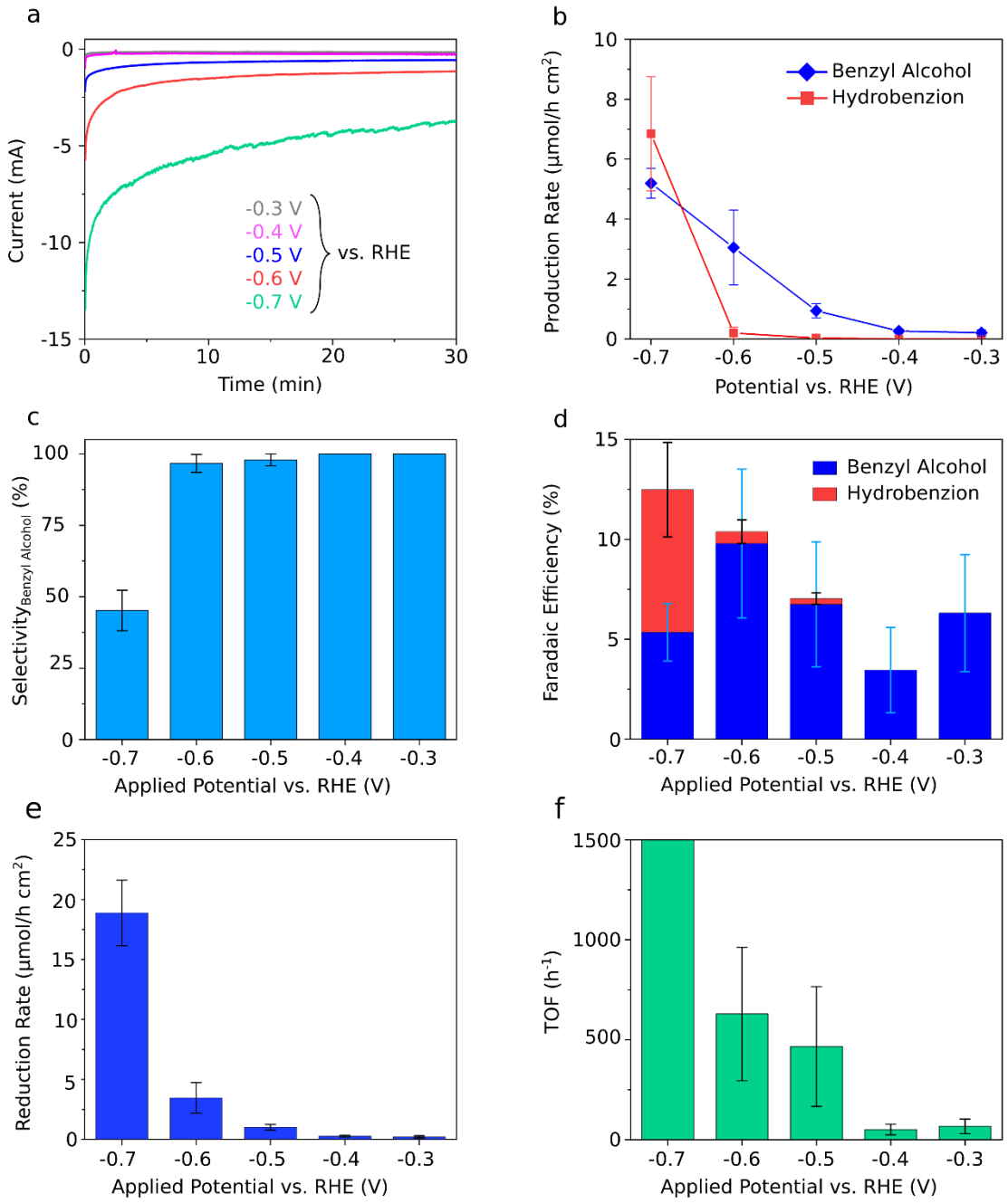

Figure 4. Results of 30 min electrolysis experiments in 0.1 M H_2SO_4 with 20 mM benzaldehyde at 25° C with 500 rpm stirring. (a) Current response of the chrono amperometry at different potentials. (b) Production rate for benzyl alcohol and hydrobenzoin on MoS_2/anC:N_G for different applied potentials. (c) selectivity towards benzyl alcohol and (d) faradaic efficiency for benzyl alcohol and hydrobenzoin. (e) Total reduction rate of benzaldehyde and (f) turn over frequency normalised for MoS_2 loading; the full range of the production rate and the TOF is shown in Figure S8.

TOF determinations enable a comparison with other electrode materials in the literature characterized under similar conditions. **Table 1** summarises selected relevant results obtained using benzaldehyde and Pt-group metals for the ECH; potentials are all reported vs RHE for a meaningful comparison to be possible. Lopez-Ruiz et al. investigated the ECH of different organic compounds on a range of metals,[17] and reported TOF for Pd, the 'gold' standard of ECH catalysts, of *ca.* 500 h^{-1}. This is comparable to the performance of MoS_2/anC:N_G heterostructured electrodes in this work, which yielded 468 h^{-1} and 612 h^{-1} at -0.5 and -0.6 V vs. RHE, respectively. While Lopez- Ruiz et al. report higher faradaic efficiencies, we note that the reaction conditions differ in the electrolyte composition and in the use by the authors of porous M/C electrocatalysts. Nonetheless, a comparison with their work suggests that MoS_2 could provide competitive performances relative to Pt-group metals. Lercher and co-workers have investigated the ECH of benzaldehyde in acetate buffer using a range of Pt-group metals supported on carbon and found TOFs from <500 h^{-1} up to *ca*. 4000 h^{-1} depending on applied potential and metal.[20, 52] While their TOF values are higher compared to the ones reported in this work, they were obtained at pH 5 which would suppress the HER compared to pH 1, as used in our work. Results in Table 1 indicate that an overpotential of *ca.* 500 mV is needed to achieve comparable TOF between conventional Pd/C and MoS_2/anC:N_G while, given the same applied potential, the TOF at MoS_2 is typically ~25% that observed at Pd/C. Given that Pd prices are *ca.*500-fold higher than those of Mo,[53] the performance of the MoS_2/anC:N_G appears promising for applications that would benefit from low materials costs, such as the valorization of mixed bioresource feeds.

Table 1. Selected TOF values reported in literature for the ECH of benzaldehyde using Pt-group metals, compared to those of MoS_2/anC:N_G in this work. All potentials are reported vs RHE to facilitate comparison.

Material	Substrate	Electrolyte	Potential	TOF_{ECH} (h^{-1})	Ref.
MoS_2/anC:N_G	Benzaldehyde 20 mM	0.1 M H_2SO_4	-0.5 V_{RHE} -0.6 V_{RHE}	468 612	This work
Pd Ru	Benzaldehyde 80 mM	47.5% IPA, 47.5 H_2O, 5% AcOH (est. pH 2.4)[a]	-0.8 V_{RHE}	~500 ~200	[17]
Pd/C Rh/C Pt/C	Benzaldehyde 20 mM	Acetate buffer pH 5[a]	-0.5 V_{RHE}	~4000 ~2000 ~2000	[20]
Pd/C Rh/C Ru/C	Benzaldehyde 20 mM	3 M Acetate buffer pH 5.2	-0.1 V_{RHE}	~500 ~350 ~250	[52]

a – values of potential vs RHE used for the comparison are estimated based on the pH value indicated in the corresponding reference.

It is further interesting to discuss the significant decrease in selectivity observed in our results at -0.7 V vs RHE. The data in **Figure 4b** shows that although production rates of benzyl alcohol steadily increase vs cathodic overpotential, below -0.6 V vs RHE there is a sharp increase in electro-dimerization rates that suggests a possible change in reaction pathway/s at this potential. We propose that this is the result of direct reduction, which is known to compete with surface-catalysed hydrogenations,[16, 28, 54] becoming a fast reaction below this threshold potential. Cantu et al. investigated the potential-dependent free energy of intermediate species involved in reaction pathways for the reduction of benzaldehyde, at a range of metal surfaces and on carbon.[16] According to the authors, at more anodic potentials a concerted reaction mechanism is favoured, involving the equivalent of H_{ads} addition to the organic adsorbate. For more cathodic overpotentials, a sequential electron-proton transfer offers instead a lower free energy pathway, with the potential depending on the electrode material used (**Scheme S1**). This sequential pathway can compete with surface-mediated H_{ads} addition,[28, 54] and proceeds via

reduction of the organic substrate at the electrode followed by protonation from solution. Lessard's early work had already highlighted the difference between electrocatalytic hydrogenation and a reaction pathway they call electronation-protonation,[55] that is available on most electrodes at sufficiently high overpotentials. The sequential pathway increases the rate of ketyl radical formation,[28, 54] which we believe explains the greater rate of production for dimerization products at the highest overpotential tested in our experiments.

Finally, the scope of ECH at MoS_2/carbon heterostructured electrodes was expanded to furfural, an unsaturated organic of great interest for biomass valorization using ECH.[27, 39] Electrolysis studies were carried out using the same setup as for benzaldehyde using an electrolysis time of 1 h; the resulting descriptors for the ECH of furfural are shown in **Figure 5**. The production rate (**Figure 5a**) of the alcohol increases with increased cathodic potential. Similarly to the results for benzaldehyde, at higher cathodic potentials the dimerization reaction can be observed. These production rates translate into TOF of up to 930 h^{-1} at -0.6 V vs. RHE (**Figure 5b**). While the selectivity and the production rate towards the alcohol product are high, the observed FE remain relatively low (**Figure 5c**). Given that the mass balance was comparable to that obtained using benzaldehyde (**Figure S8**), the low FE values are likely the result of competition from the HER.

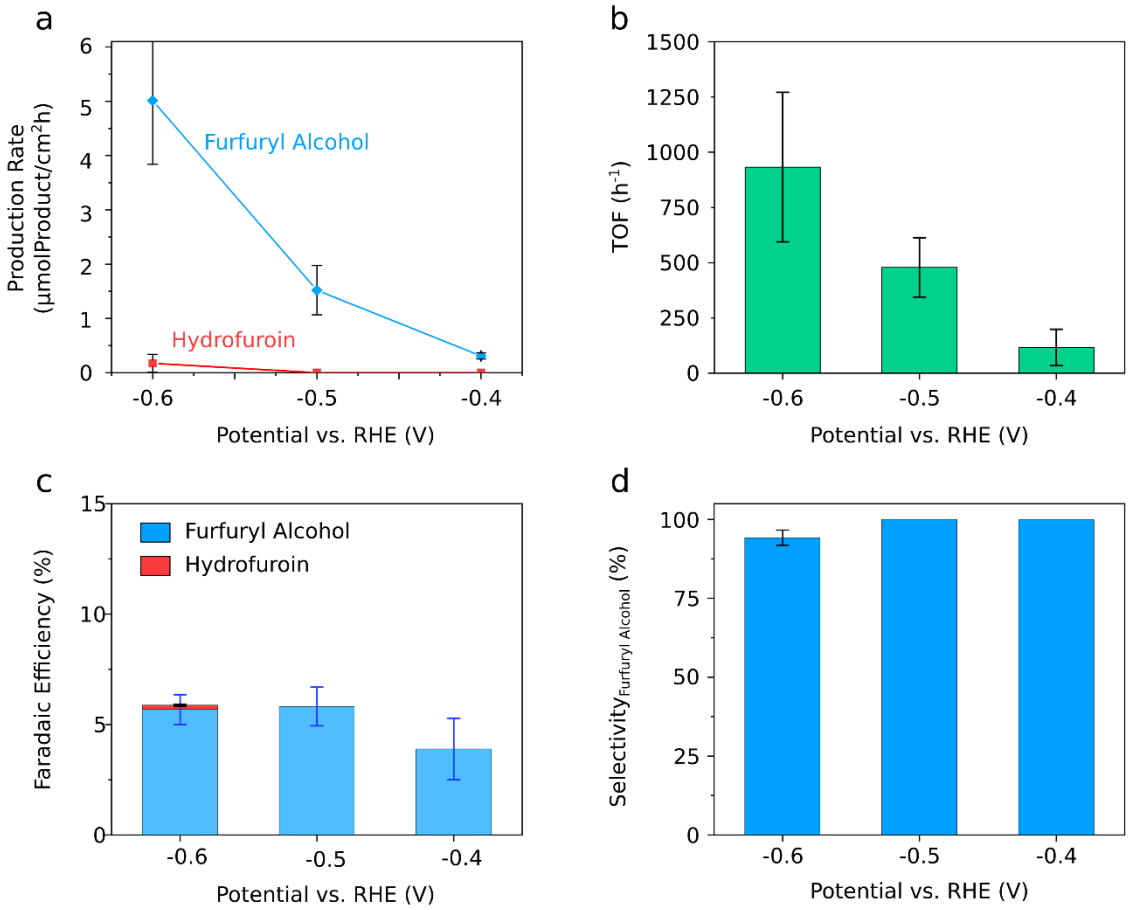

Figure 5. Results of 60 min electrolysis experiments in 0.1 M H_2SO_4 with 20 mM furfural at 25° C with 500 rpm stirring. (a) Production rate for furfuryl alcohol and hydrofuroin on MoS_2/anC:N_G for different applied potentials (b) turn over frequency normalised for MoS_2 loading. (c) faradaic efficiency for furfuryl alcohol and hydrofuroin (d) selectivity towards furfuryl alcohol.

The resulting descriptors for the ECH of benzaldehyde and furfural are summarized in **Table 2**. It can be seen that descriptors for both organics are comparable and follow similar trends, indicating the same underlying reasoning for the results as for benzaldehyde. The FE and selectivity of the ECH of furfural on MoS_2/anC:N_G are in a similar range to other values reported in literature for other MoS_2-based electrode materials. Huang et al.[35] reported on the ECH of furfural on electrodeposited MoS_2 using galvanostatic experiments; the selectivity and the FE values estimated based on their experimental conditions are comparable to those observed in this work. Notably, the planar geometry of our heterostructured electrodes enabled

for the first time to calculate estimates of TOF for MoS_2, which are comparable or higher relative to those reported for the ECH of furfural at a range of precious metal electrodes, where also relatively low FE were reported.[17, 56] The mass balance of experiments summarised in **Figure 5** was *ca.* 95%, (**Figure S8**); this is in contrast to several reports in the furfural ECH literature, where problems with mass balance closure are well recognised and attributed to side reactions.[26, 27, 39, 57] Notably, no products arising from ring hydrogenation were observed, despite the furan ring being more amenable to hydrogenation compared to the benzene ring of benzaldehyde. This indicates that the chemoselectivity of the ECH that was observed with benzaldehyde is also valid for the ECH of furfural at least under the electrolysis conditions explored in these experiments.

Table 2. Comparison of performance indicators obtained from electrolysis experiments using benzaldehyde and furfural (20 mM organic, 0.1 M H_2SO_4, 500 rpm stirring at 25 °C) as the organic substrate of the ECH.

	Applied Potential (V vs. RHE)	**Benzaldehyde**	**Furfural**
F.E. (Total) (%)	-0.4	3.5 ± 2.1	3.9 ± 1.4
	-0.5	7.0 ± 3.1	5.8 ± 0.9
	-0.6	10.4 ± 3.8	6.0 ± 0.6
Selectivity (Alcohol) (%)	-0.4	100	100
	-0.5	97.9 ± 2.1	100
	-0.6	96.7 ± 3.1	94.2 ± 2.4
Production Rate (Alcohol) ($\mu mol\ cm^{-2}\ h^{-1}$)	-0.4	0.3 ± 0.1	0.3 ± 0.1
	-0.5	1.0 ± 0.2	1.5 ± 0.5
	-0.6	3.1 ± 1.2	5.0 ± 1.2
TOF (h^{-1})	-0.4	51 ± 27	$(1.2 \pm 0.8)\times10^2$
	-0.5	$(5 \pm 3)\times10^2$	$(4.8 \pm 1.3)\times10^2$
	-0.6	$(6.2 \pm 3.3)\times10^2$	$(9 \pm 3)\times10^2$

Conclusion

We report on the synthesis of MoS_2 thin film nanoparticle electrodes onto graphitized nitrogenated carbon supports via a CVD proximity synthetic strategy. The thin film architecture enables quantitative characterization of the electroactive MoS_2 loading while their simple

geometry ensures well defined mass transport. The ECH of benzaldehyde was investigated first via voltammetry and then using potentiostatic electrolysis experiments followed by product analysis. We find that under the experimental conditions explored it is possible to generate the alcohol product with high selectivity at modest overpotentials. At high cathodic overpotentials, the rate of electrodimerization to hydrobenzoin is observed to increase abruptly to the detriment of the alcohol faradaic efficiency. We speculate that this is due to direct reduction followed by protonation becoming an important competing reaction at the most cathodic overpotentials tested.

The application of the heterostructures was further expanded to furfural, a bio-derived compound whose hydrogenation is of particular interest for applications including fuels, resins and plasticizers. At the investigated conditions similar results compared to the reaction with benzaldehyde were found. The production rates and turn over frequencies observed are competitive with those at conventional precious metal catalysts. The relatively low faradaic efficiency observed could be addressed by changing the reaction conditions, namely increasing the pH, to suppress the HER and potentially favour the ECH.

Notably, we report for the first time determinations of TOF for ECH at MoS_2 materials. This enabled a quantitative comparison and benchmarking of the performance of this HER-active material against other common Pt-group metal electrocatalysts. We find that MoS_2/N-carbon offers attractive performances that can be comparable to those of selected Pt/C or Pd/C examples in the literature and only *ca.* 25% lower than some of the best performances reported for such precious metals. These experiments demonstrated that high selectivity towards the alcohol could be achieved at moderate potentials while maintaining a similar TOF as observed with benzaldehyde. Overall, results suggest that MoS_2 could be an attractive replacement and possibly offer overall lower materials costs for implementation of ECH at scale. Studies using 2-electrode flow electrolyser devices and mixed organic feeds might be therefore desirable and

justified to further assess the performances of these materials in applications to biomass valorization at scale.

Supporting Information

The Supporting Information is available free of charge at *https:xxx.xxx.xxx*. Additional TEM analysis, XRD analysis, XPS analysis, voltammetry characterization, control electrolysis experiments, representative chromatograms, post-mortem Raman characterization, ECH figures of merit and schemes of reaction pathways.

Acknowledgements

This publication has emanated from research conducted with the financial support of Taighde Éireann – Research Ireland under Grant number 19/FFP/6761 and GOIPG/2023/4653. NH also received funding from the European Union's Horizon 2020 research and innovation program under the Marie Skłodowska-Curie Grant Agreement No. 713567 (EDGE-Project HECAT4H2). The results of this publication reflect only the authors' view and the Commission is not responsible for any use that may be made of the information it contains. The authors are grateful to Dr. N. McEvoy for support with CVD instrumentation. TEM imaging was carried out at the Advanced Microscopy Laboratory (AML) at the AMBER Research Centre, Trinity College Dublin, Ireland; we are grateful to Dr. R. Bekarevich and C. Downing for assistance with TEM. We are thankful to Dr. B. Twamley for assistance with XRD. Use of the XPS of I. V. Shvets and C. McGuinness provided under SFI Equipment Infrastructure funds.

References

1. Akhade, S. A.; Singh, N.; Gutierrez, O. Y.; Lopez-Ruiz, J.; Wang, H.; Holladay, J. D.; Liu, Y.; Karkamkar, A.; Weber, R. S.; Padmaperuma, A. B.; Lee, M. S.; Whyatt, G.

A.; Elliott, M.; Holladay, J. E.; Male, J. L.; Lercher, J. A.; Rousseau, R.; Glezakou, V. A., Electrocatalytic Hydrogenation of Biomass-Derived Organics: A Review. *Chem Rev* **2020,** *120* (20), 11370-11419.

2. Kwon, Y.; Birdja, Y. Y.; Raoufmoghaddam, S.; Koper, M. T., Electrocatalytic hydrogenation of 5-hydroxymethylfurfural in acidic solution. *ChemSusChem* **2015,** *8* (10), 1745-51.

3. Lam, C. H.; Das, S.; Erickson, N. C.; Hyzer, C. D.; Garedew, M.; Anderson, J. E.; Wallington, T. J.; Tamor, M. A.; Jackson, J. E.; Saffron, C. M., Towards sustainable hydrocarbon fuels with biomass fast pyrolysis oil and electrocatalytic upgrading. *Sustain. Energy Fuels* **2017,** *1* (2), 258-266.

4. Wijaya, Y. P.; Smith, K. J.; Kim, C. S.; Gyenge, E. L., Electrocatalytic hydrogenation and depolymerization pathways for lignin valorization: toward mild synthesis of chemicals and fuels from biomass. *Green Chem.* **2020,** *22* (21), 7233-7264.

5. Orella, M. J.; Román-Leshkov, Y.; Brushett, F. R., Emerging opportunities for electrochemical processing to enable sustainable chemical manufacturing. *Curr. Opin. Chem. Eng.* **2018,** *20*, 159-167.

6. Meemken, F.; Baiker, A., Recent Progress in Heterogeneous Asymmetric Hydrogenation of C═O and C═C Bonds on Supported Noble Metal Catalysts. *Chem. Rev.* **2017,** *117* (17), 11522-11569.

7. Chen, B.; Dingerdissen, U.; Krauter, J. G. E.; Lansink Rotgerink, H. G. J.; Möbus, K.; Ostgard, D. J.; Panster, P.; Riermeier, T. H.; Seebald, S.; Tacke, T.; Trauthwein, H., New developments in hydrogenation catalysis particularly in synthesis of fine and intermediate chemicals. *Appl. Catal., A* **2005,** *280* (1), 17-46.

8. Gil, A.; Sancho-Sanz, I.; Korili, S. A., Progress and Perspectives in the Catalytic Hydrotreatment of Bio-Oils: Effect of the Nature of the Metal Catalyst. *Ind. Eng. Chem. Res.* **2024,** *63* (27), 11759-11775.

9. Lessard, J., Electrocatalytic Hydrogenation. In *Encyclopedia of Applied Electrochemistry*, Kreysa, G.; Ota, K.-i.; Savinell, R. F., Eds. Springer New York: New York, NY, 2014; pp 443-448.

10. Zhao, B.-H.; Chen, F.; Wang, M.; Cheng, C.; Wu, Y.; Liu, C.; Yu, Y.; Zhang, B., Economically viable electrocatalytic ethylene production with high yield and selectivity. *Nat. Sustain.* **2023,** *6* (7), 827-837.

11. Hochman, G.; Goldman, A. S.; Felder, F. A.; Mayer, J. M.; Miller, A. J. M.; Holland, P. L.; Goldman, L. A.; Manocha, P.; Song, Z.; Aleti, S., Potential Economic Feasibility of Direct Electrochemical Nitrogen Reduction as a Route to Ammonia. *ACS Sustain. Chem. Eng.* **2020,** *8* (24), 8938-8948.

12. Bruch, Q. J.; Connor, G. P.; McMillion, N. D.; Goldman, A. S.; Hasanayn, F.; Holland, P. L.; Miller, A. J. M., Considering Electrocatalytic Ammonia Synthesis via Bimetallic Dinitrogen Cleavage. *ACS Catal.* **2020,** *10* (19), 10826-10846.

13. Qing, G.; Ghazfar, R.; Jackowski, S. T.; Habibzadeh, F.; Ashtiani, M. M.; Chen, C.-P.; Smith, M. R., III; Hamann, T. W., Recent Advances and Challenges of Electrocatalytic N_2 Reduction to Ammonia. *Chem. Rev.* **2020,** *120* (12), 5437-5516.

14. Chen, H.; Iyer, J.; Liu, Y.; Krebs, S.; Deng, F.; Jentys, A.; Searles, D. J.; Haider, M. A.; Khare, R.; Lercher, J. A., Mechanism of Electrocatalytic H_2 Evolution, Carbonyl Hydrogenation, and Carbon–Carbon Coupling on Cu. *J. Am. Chem. Soc.* **2024,** *146* (20), 13949-13961.

15. Andrews, E.; Lopez-Ruiz, J. A.; Egbert, J. D.; Koh, K.; Sanyal, U.; Song, M.; Li, D.; Karkamkar, A. J.; Derewinski, M. A.; Holladay, J.; Gutiérrez, O. Y.; Holladay, J. D., Performance of Base and Noble Metals for Electrocatalytic Hydrogenation of Bio-Oil-Derived Oxygenated Compounds. *ACS Sustain. Chem. Eng.* **2020,** *8* (11), 4407-4418.

16. Cantu, D. C.; Padmaperuma, A. B.; Nguyen, M.-T.; Akhade, S. A.; Yoon, Y.; Wang, Y.-G.; Lee, M.-S.; Glezakou, V.-A.; Rousseau, R.; Lilga, M. A., A Combined Experimental and Theoretical Study on the Activity and Selectivity of the Electrocatalytic Hydrogenation of Aldehydes. *ACS Catal.* **2018,** *8* (8), 7645-7658.

17. Lopez-Ruiz, J. A.; Andrews, E.; Akhade, S. A.; Lee, M.-S.; Koh, K.; Sanyal, U.; Yuk, S. F.; Karkamkar, A. J.; Derewinski, M. A.; Holladay, J.; Glezakou, V.-A.; Rousseau, R.; Gutiérrez, O. Y.; Holladay, J. D., Understanding the Role of Metal and Molecular Structure on the Electrocatalytic Hydrogenation of Oxygenated Organic Compounds. *ACS Catal.* **2019,** *9* (11), 9964-9972.

18. Sanyal, U.; Lopez-Ruiz, J.; Padmaperuma, A. B.; Holladay, J.; Gutiérrez, O. Y., Electrocatalytic Hydrogenation of Oxygenated Compounds in Aqueous Phase. *Org. Process Res. Dev.* **2018,** *22* (12), 1590-1598.

19. Singh, N.; Sanyal, U.; Ruehl, G.; Stoerzinger, K. A.; Gutiérrez, O. Y.; Camaioni, D. M.; Fulton, J. L.; Lercher, J. A.; Campbell, C. T., Aqueous phase catalytic and electrocatalytic hydrogenation of phenol and benzaldehyde over platinum group metals. *J. Catal.* **2020,** *382*, 372-384.

20. Song, Y.; Sanyal, U.; Pangotra, D.; Holladay, J. D.; Camaioni, D. M.; Gutiérrez, O. Y.; Lercher, J. A., Hydrogenation of benzaldehyde via electrocatalysis and thermal catalysis on carbon-supported metals. *J. Catal.* **2018,** *359*, 68-75.

21. Villalba, M.; del Pozo, M.; Calvo, E. J., Electrocatalytic hydrogenation of acetophenone and benzophenone using palladium electrodes. *Electrochim. Acta* **2015,** *164*, 125-131.

22. Sanyal, U.; Koh, K.; Meyer, L. C.; Karkamkar, A.; Gutiérrez, O. Y., Simultaneous electrocatalytic hydrogenation of aldehydes and phenol over carbon-supported metals. *J. Appl. Electrochem.* **2020,** *51* (1), 27-36.

23. Anibal, J.; Malkani, A.; Xu, B., Stability of the ketyl radical as a descriptor in the electrochemical coupling of benzaldehyde. *Catal Sci Technol* **2020,** *10* (10), 3181-3194.

24. Zheng, M.; Zhang, J.; Wang, P.; Jin, H.; Zheng, Y.; Qiao, S.-Z., Recent Advances in Electrocatalytic Hydrogenation Reactions on Copper-Based Catalysts. *Adv. Mater.* **2024,** *36* (14), 2307913.

25. Yu, J.; Zhang, P.; Li, L.; Li, K.; Zhang, G.; Liu, J.; Wang, T.; Zhao, Z.-J.; Gong, J., Electroreductive coupling of benzaldehyde by balancing the formation and dimerization of the ketyl intermediate. *Nat. Commun.* **2022,** *13* (1), 7909.

26. Jung, S.; Biddinger, E. J., Electrocatalytic Hydrogenation and Hydrogenolysis of Furfural and the Impact of Homogeneous Side Reactions of Furanic Compounds in Acidic Electrolytes. *ACS Sustain. Chem. Eng.* **2016,** *4* (12), 6500-6508.

27. Jung, S.; Biddinger, E. J., Controlling Competitive Side Reactions in the Electrochemical Upgrading of Furfural to Biofuel. *Energy Technology* **2018,** *6* (7), 1370-1379.

28. Chadderdon, X. H.; Chadderdon, D. J.; Matthiesen, J. E.; Qiu, Y.; Carraher, J. M.; Tessonnier, J.-P.; Li, W., Mechanisms of Furfural Reduction on Metal Electrodes: Distinguishing Pathways for Selective Hydrogenation of Bioderived Oxygenates. *J. Am. Chem. Soc.* **2017,** *139* (40), 14120-14128.

29. Liu, H.; Patel, D. M.; Chen, Y.; Lee, J.; Lee, T.-H.; Cady, S. D.; Cochran, E. W.; Roling, L. T.; Li, W., Unraveling electroreductive mechanisms of biomass-derived aldehydes via tailoring interfacial environments. *ACS Catal.* **2022,** *12* (22), 14072-14085.

30. Zhang, X.; Liu, B.; Wang, Y.; Long, Y.; Xu, Z.; Lin, H.-T.; Luque, R.; Yan, K., Efficient radical-driving electrocatalytic dimerization of furfural to jet fuel precursors using WMoB nanoflakes. *Green Chem.* **2025**.

31. Bonde, J.; Moses, P. G.; Jaramillo, T. F.; Nørskov, J. K.; Chorkendorff, I., Hydrogen evolution on nano-particulate transition metal sulfides. *Faraday Discuss.* **2009,** *140* (0), 219-231.

32. Cao, Y., Roadmap and Direction toward High-Performance MoS2 Hydrogen Evolution Catalysts. *ACS Nano* **2021,** *15* (7), 11014-11039.

33. Liu, G.; Ding, L.; Meng, Y.; Ali, A.; Zuo, G.; Meng, X.; Chang, K.; Li, O. L.; Ye, J., A review on ultra-small undoped MoS_2 as advanced catalysts for renewable fuel production. *Carbon Energy* **2024,** *6* (2), e521.

34. Ren, H.-D.; Lang, Z.-L.; Tan, H.-Q.; Wang, Y.-H.; Li, Y.-G., p-Block Single-Atom Anchored MoS_2 Monolayer for Efficient Electroreduction of CO_2 to Formate via Strong p–sp Interaction. *J. Phys. Chem. C* **2024,** *128* (16), 6702-6710.

35. Huang, S.; Jin, Y.; Zhang, M.; Yan, K.; Feng, S.-P.; Lam, J. C.-H., MoS_2-catalyzed selective electrocatalytic hydrogenation of aromatic aldehydes in an aqueous environment. *Green Chem.* **2022,** *24* (20), 7974-7987.

36. Nolan, H.; Schröder, C.; Brunet-Cabré, M.; Pota, F.; McEvoy, N.; McKelvey, K.; Perova, T. S.; Colavita, P. E., MoS_2/carbon heterostructured catalysts for the hydrogen evolution reaction: N-doping modulation of substrate effects in acid and alkaline electrolytes. *Carbon* **2023,** *202*, 70-80.

37. Pota, F.; Costa de Oliveira, M. A.; Schröder, C.; Brunet Cabré, M.; Nolan, H.; Rafferty, A.; Jeannin, O.; Camerel, F.; Behan, J. A.; Barrière, F.; Colavita, P. E., Porous N-

Doped Carbon-encapsulated Iron as Novel Catalyst Architecture for the Electrocatalytic Hydrogenation of Benzaldehyde. *ChemSusChem* **2025,** *18* (1), e202400546.

38. Koh, K.; Sanyal, U.; Lee, M.-S.; Cheng, G.; Song, M.; Glezakou, V.-A.; Liu, Y.; Li, D.; Rousseau, R.; Gutiérrez, O. Y.; Karkamkar, A.; Derewinski, M.; Lercher, J. A., Electrochemically Tunable Proton-Coupled Electron Transfer in Pd-Catalyzed Benzaldehyde Hydrogenation. *Angew. Chem. Int. Ed.* **2020,** *59* (4), 1501-1505.

39. Li, Z.; Kelkar, S.; Lam, C. H.; Luczek, K.; Jackson, J. E.; Miller, D. J.; Saffron, C. M., Aqueous electrocatalytic hydrogenation of furfural using a sacrificial anode. *Electrochim. Acta* **2012,** *64*, 87-93.

40. Cabré, M. B.; Schröder, C.; Pota, F.; de Oliveira, M. A. C.; Nolan, H.; Henderson, L.; Brazel, L.; Spurling, D.; Nicolosi, V.; Martinuz, P.; Longhi, M.; Amargianou, F.; Bärmann, P.; Petit, T.; McKelvey, K.; Colavita, P. E., Carbon Thin-Film Electrodes as High-Performing Substrates for Correlative Single Entity Electrochemistry. *Small Methods* **2025,** *9* (1), 2400639.

41. O'Brien, M.; McEvoy, N.; Hallam, T.; Kim, H.-Y.; Berner, N. C.; Hanlon, D.; Lee, K.; Coleman, J. N.; Duesberg, G. S., Transition Metal Dichalcogenide Growth via Close Proximity Precursor Supply. *Sci. Rep.* **2014,** *4* (1), 7374.

42. Radisavljevic, B.; Radenovic, A.; Brivio, J.; Giacometti, V.; Kis, A., Single-layer MoS_2 transistors. *Nat. Nanotechnol.* **2011,** *6* (3), 147-150.

43. Pimenta, M. A.; del Corro, E.; Carvalho, B. R.; Fantini, C.; Malard, L. M., Comparative Study of Raman Spectroscopy in Graphene and MoS_2-type Transition Metal Dichalcogenides. *Acc. Chem. Res.* **2015,** *48* (1), 41-47.

44. Yu, Y.; Nam, G.-H.; He, Q.; Wu, X.-J.; Zhang, K.; Yang, Z.; Chen, J.; Ma, Q.; Zhao, M.; Liu, Z.; Ran, F.-R.; Wang, X.; Li, H.; Huang, X.; Li, B.; Xiong, Q.; Zhang, Q.; Liu, Z.; Gu, L.; Du, Y.; Huang, W.; Zhang, H., High phase-purity 1T′-MoS_2- and 1T′-$MoSe_2$-layered crystals. *Nature Chem.* **2018,** *10* (6), 638-643.

45. Spevack, P. A.; McIntyre, N. S., Thermal reduction of molybdenum trioxide. *J. Phys. Chem.* **1992,** *96* (22), 9029-9035.

46. Jing, Y.; Tan, X.; Zhou, Z.; Shen, P., Tuning electronic and optical properties of MoS_2 monolayer via molecular charge transfer. *J. Mater. Chem. A* **2014,** *2* (40), 16892-16897.

47. Wakabayashi, N.; Smith, H. G.; Nicklow, R. M., Lattice dynamics of hexagonal MoS_2 studied by neutron scattering. *Phys. Rev. B* **1975,** *12* (2), 659-663.

48. Ioroi, T.; Fujiwara, N.; Siroma, Z.; Yasuda, K.; Miyazaki, Y., Platinum and molybdenum oxide deposited carbon electrocatalyst for oxidation of hydrogen containing carbon monoxide. *Electrochem. Commun.* **2002,** *4* (5), 442-446.

49. Wang, Y.; Fachini, E. R.; Cruz, G.; Zhu, Y.; Ishikawa, Y.; Colucci, J. A.; Cabrera, C. R., Effect of Surface Composition of Electrochemically Codeposited Platinum/Molybdenum Oxide on Methanol Oxidation. *J. Electrochem. Soc.* **2001,** *148* (3), C222.

50. Brennan, M. P. J.; Brown, O. R., Carbon electrodes: Part 1. Hydrogen evolution in acidic solution. *J. Appl. Electrochem.* **1972,** *2* (1), 43-49.

51. Dabo, P.; Brossard, L.; Me´nard, H.; Tremblay, P., Hydrogen activation of spectroscopic graphite surface by argon plasma etching. *J. Appl. Electrochem.* **1998,** *28* (6), 601-606.

52. Sanyal, U.; Yuk, S. F.; Koh, K.; Lee, M. S.; Stoerzinger, K.; Zhang, D.; Meyer, L. C.; Lopez-Ruiz, J. A.; Karkamkar, A.; Holladay, J. D., Hydrogen bonding enhances the electrochemical hydrogenation of benzaldehyde in the aqueous phase. *Angew. Chem.* **2021,** *133* (1), 294-300.

53. Page, W. https://www.dailymetalprice.com and https://www.metal.com/. (accessed 15/08/2025).

54. Kundu, B. K.; Sun, Y., Electricity-driven organic hydrogenation using water as the hydrogen source. *Chem. Sci.* **2024,** *15* (40), 16424-16435.

55. Chan-Shing, E. S.; Boucher, D.; Lessard, J., The electrochemical reduction of α-nitrocumene in a protic and basic medium on large surface area (porous) electrodes: electronation-protonation or electrocatalytic hydrogenation? *Can. J. Chem.* **1999,** *77* (5-6), 687-694.

56. Sanyal, U.; Koh, K.; Meyer, L. C.; Karkamkar, A.; Gutiérrez, O. Y., Simultaneous electrocatalytic hydrogenation of aldehydes and phenol over carbon-supported metals. *J. Appl. Electrochem.* **2021,** *51* (1), 27-36.

57. May, A. S.; Biddinger, E. J., Strategies to Control Electrochemical Hydrogenation and Hydrogenolysis of Furfural and Minimize Undesired Side Reactions. *ACS Catal.* **2020,** *10* (5), 3212-3221.